NOTES

Magnetic Resonance in Medicine 56:198–203 (2006)

Reducing Gradient Imperfections for Spiral Magnetic Resonance Spectroscopic Imaging

Dong-Hyun Kim[1*] and Daniel M. Spielman[2]

Spiral *k*-space magnetic resonance spectroscopic imaging (MRSI) requires high performance from gradient hardware systems. During the readout phase, oscillating gradients are continuously played out, which can cause undesired effects. These effects on the quality of SI data are non-intuitive because of their time-varying nature. In this work we describe the effects of undesirable gradient performance on SI. Measurements of the true readout trajectories were performed and the results were then used in the reconstruction process. The effects of these imperfections resulted in a spatially and spectrally varying amplitude and frequency modulation. The use of the measured trajectories in the reconstruction process yielded an up to 20% increase in signal amplitude recovery. Magn Reson Med 56: 198–203, 2006. © 2006 Wiley-Liss, Inc.

Key words: magnetic resonance spectroscopic imaging; spiral readout gradients; gradient imperfections; eddy currents; spiral CSI

Spiral-based magnetic resonance spectroscopic imaging (MRSI) provides unique advantages for chemical shift imaging (CSI) (1). The spatial *k*-space is sampled in a spiral fashion, while data along the spectral dimension are acquired by repeating the spiral lobes. With this sampling scheme, the total minimum scan time required to collect the *k*-space data points is significantly reduced compared to conventional phase-encoded approaches.

During the readout phase of a spiral MRSI scheme, the gradients are designed to continuously play out a spiral *k*-space readout trajectory form. For example, 256 or 512 spiral lobes can be executed during one readout period. Each spiral lobe goes out in *k*-space and subsequently quickly returns back to the (k_x, k_y) origin via gradient trajectories termed rewinders. The presence of undesirable effects due to gradient imperfections arising from eddy currents, nonlinear gradient amplifier response function, gradient infidelity issues, or even mechanical vibrations can cause the desired spiral *k*-space trajectory to deviate from its original design and introduce time-varying B_0 variations. The effects of these undesirable properties on SI data are non-intuitive because these terms vary with time during the readout period. To elucidate these effects, a means of measuring the true trajectory for the duration of the readout must be implemented and studied. Several different *k*-space trajectory measurement schemes, most of which focus on MRI applications, have been proposed (2–7).

Modern gradient systems are equipped with eddy-current compensation (preemphasis) systems; however, these systems are not perfect, and they mostly compensate for certain ranges of time constants (8,9). In addition to the *k*-space distortions, main field variations can cause problems for spectroscopic applications (10). To overcome eddy-current-induced main field drift, a separate water referencing acquisition is commonly used to eliminate the time-varying phase accumulations (11). For SI using oscillating readout gradients, both *k*-space and main field variations can influence the quality of the reconstructed data. It is therefore beneficial to obtain simultaneously the *k*-space trajectory and the main field deviations. In a previous study (12) we provided the preliminary results of these measurements; however, the approach at that time was limited to measuring only the *k*-space trajectory from small portions of the entire readout cycle. In addition, the study did not show the resulting effects of these gradient imperfections, and no compensation method was provided.

In this work we describe the effect of distorted trajectories on spiral MRSI data. An efficient method for measuring the trajectory is illustrated that is intended to measure the *k*-space trajectory and main field perturbations due to gradient imperfections for the duration of the entire readout period. Simulations were performed using these measured trajectories to identify different distortion characteristics. Finally, we show that the spectral data quality can be enhanced by reconstructing spiral MRSI data using the measured trajectory.

MATERIALS AND METHODS

Spiral readout gradients were implemented in a point-resolved spectroscopy (PRESS) sequence. The gradient waveforms were designed using analytic expressions, which permitted a variety of different trajectories to be generated and tested (13). In particular, the trajectory with the following design parameters was used for simulations and corrections: 1-ms spiral lobe including rewinders (= 1000 Hz spectral bandwidth), 512 spiral lobes (= 512 ms readout period), 16 × 16 matrix size, 16-cm FOV, and four spatial interleaves in k_{xy}. All other spiral waveforms were designed for a 1-cc resolution for different FOVs and tested

[1]Department of Radiology, University of California–San Francisco, San Francisco, California, USA

[2]Department of Radiology, Stanford University, Stanford, California, USA

Grant sponsor: NIH; Grant numbers: CA48269; RR09784.

*Correspondence to: Dong-Hyun Kim, Ph.D., Department of Radiology, University of California–San Francisco, Campus Box 0628, San Francisco, CA 94143. E-mail: donghyun.kim@radiology.ucsf.edu

Received 12 October 2005; revised 16 February 2006; accepted 20 March 2006.

DOI 10.1002/mrm.20928

Published online 24 May 2006 in Wiley InterScience (www.interscience.wiley.com).

on a 1.5 T or a 3 T GE Signa EXCITE scanner (General Electric Healthcare Technologies, Waukesha, WI, USA) with a maximum gradient strength of 40 mT/m and maximum slew rate of 150 mT/m/ms (software release 11.0).

The spiral trajectories were measured using an extension of the approach proposed by Duyn et al. (7). Instead of using a slice-select slab for excitation, we excited small voxels (~1 cc) that were randomly chosen from a water phantom (diameter = 22 cm) placed within the scanner. Small voxels are readily prescribed and excited using the PRESS scheme. For each small voxel selected, three measurements were performed by setting $g_x(t) = 0$, $g_y(t) = 0$, and $g_x(t) = g_y(t) = 0$. Sixteen averages were obtained per voxel for a scan time of 4 min (TR/TE = 2000/130 ms).

The signal acquired can be approximated by

$$s(t) \approx \int m(x,y) e^{i[2\pi k_x(t)x + 2\pi k_y(t)y + \Delta b(t)]} d(x,y). \quad [1]$$

m(x,y) is the spin magnetization which can be approximated by a delta function, $m(x,y) \approx \delta(x - x_0, y - y_0)$, where (x_0, y_0) represent the selected voxel location. $\Delta b(t)$ represents the phase accrual due to the time-varying main field changes, i.e., $\Delta b(t) = \gamma \int \Delta B_0(\tau) d\tau$, where $\Delta B_o(t)$ represents the time-varying main magnet field. The phase of our signal can be represented as

$$\begin{aligned} \phi(t) &= 2\pi k_x(t) x_0 + \Delta b_x(t) \text{ when } g_y(t) = 0 \\ \phi(t) &= 2\pi k_y(t) y_0 + \Delta b_y(t) \text{ when } g_x(t) = 0 \end{aligned} \quad [2]$$

where $\Delta b(t) = \Delta b_x(t) + \Delta b_y(t)$. To eliminate phase due to inhomogeneity or other sources besides oscillating readout gradients, the phase is subtracted from the reference acquisition with $g_x(t) = g_y(t) = 0$. It is assumed that the errors are largely limited in the x and y directions because the oscillating gradients are executed in these axes.

From Eq. [2] the acquired phase becomes a function of the actual k-space position and main field drift. We estimated these variables by acquiring samples at various (x_0, y_0) locations. Since the equation is a linear function of position, a least-squares polynomial fitting algorithm was used to estimate $k_x(t)$, $k_y(t)$, and $\Delta b(t)$. Prior to the fitting, phase unwrapping of $\phi(t)$ was applied. After the fitting, low-pass filtering of the estimates was performed to reduce noise effects. Although in theory only two voxels need to be selected to estimate $k_x(t)$, $k_y(t)$, and $\Delta b(t)$, we collected data from at least eight different locations to ensure the robustness of the fitting. Any data that deviated heavily from the others were excluded in the least-squares fitting.

After we obtained an estimate of $k_x(t)$, $k_y(t)$, and $\Delta b(t)$, we used these values to investigate the effects on spiral SI. Simulations were performed in which the data were assumed to be acquired with these distortions, and compared with data acquired without any distortions. Water and other frequency components representing metabolites were assumed to be collected from a square box excitation region. Furthermore, we incorporated the measured distortions for both $k(t)$ and $\Delta b(t)$ into the reconstruction process to investigate whether this gave reduced artifacts. Validation studies using data collected from a phantom containing the major brain metabolites (NAA, Cr, and Cho), and in vivo were also conducted.

RESULTS

Figure 1 shows the measurement results from one of the four spatial interleaves. Figure 1a and b show the designed spiral lobe (red) overlaid with the measured spiral trajectory (blue) for two different zoom regions. In Fig. 1c the difference between the ideal designed trajectory and the measured trajectory, i.e., $k_{\text{ideal}}(t) - k_{\text{measured}}(t)$, where t is the duration of the readout interval ($0 \le t \le 512$ ms) is shown (blue) along with $k_{\text{ideal}}(t)$ (red). Similar to Fig. 1c, measurements from other spatial interleaves had a deviation from the ideal trajectory represented mostly as a drift in the k_y direction, implying a vulnerability of the gradient hardware associated with the Y channel for our scanner. Figure 1d and e show the results of $\Delta b(t)$. The phase variations caused by the main field have a fast varying component within $\pm 1°$ whose period is correlated to the length of the individual spiral waveform and also has a bulk drift of approximately $\pm 5°$ during the total readout interval.

The other spiral designs resulted in similar artifacts. In general, the severity of the trajectory distortion was correlated to the maximum slew rate used for the spiral trajectories. Using 100% of the maximum slew rate (150 mT/m/ms) available for the gradients typically resulted in increased artifacts. The data presented in this article used 82% of the maximum slew (123 mT/m/ms). By reducing the maximum slew rate used for the spirals, the demands on the gradient hardware can be reduced. However, this is achieved at the cost of lengthier spirals, which results in reduced spectral bandwidth.

Given the measured k-space trajectory, the effective gradients that have been executed can be inferred by differentiating $k_{\text{measured}}(t)$ with respect to time. Figure 2 shows an illustration of this for measured $k_x(t)$. The effective executed gradients (blue) can be seen lagging behind the actual designed gradients (red), which are intuitively correct, considering response functions due to eddy currents. This information can be useful when alternative correction methods based on precompensated gradient design are considered.

Simulation results regarding the k-space and main field distortions are shown in Fig. 3 for one spectral component. In Fig. 3a reconstruction errors representing the difference between the ideal trajectory for both acquisition and reconstruction compared to the following conditions are shown: (left) data acquired on the measured trajectory but reconstructed assuming an ideal nondistorted trajectory, i.e., without knowledge of the true trajectory; and (right) data acquired on the measured trajectory and reconstruction using the same measured distorted trajectory. It can be seen that trajectory discrepancies between acquisition and reconstruction cause spatially varying amplitude and frequency shifts (left). In addition, it can be seen that reconstruction with knowledge of the true trajectory can reduce these effects (right).

In Fig. 3b the effects of main field distortions are shown. The difference (right) in the reconstructed spectra with (middle) and without (left) main field distortion compen-

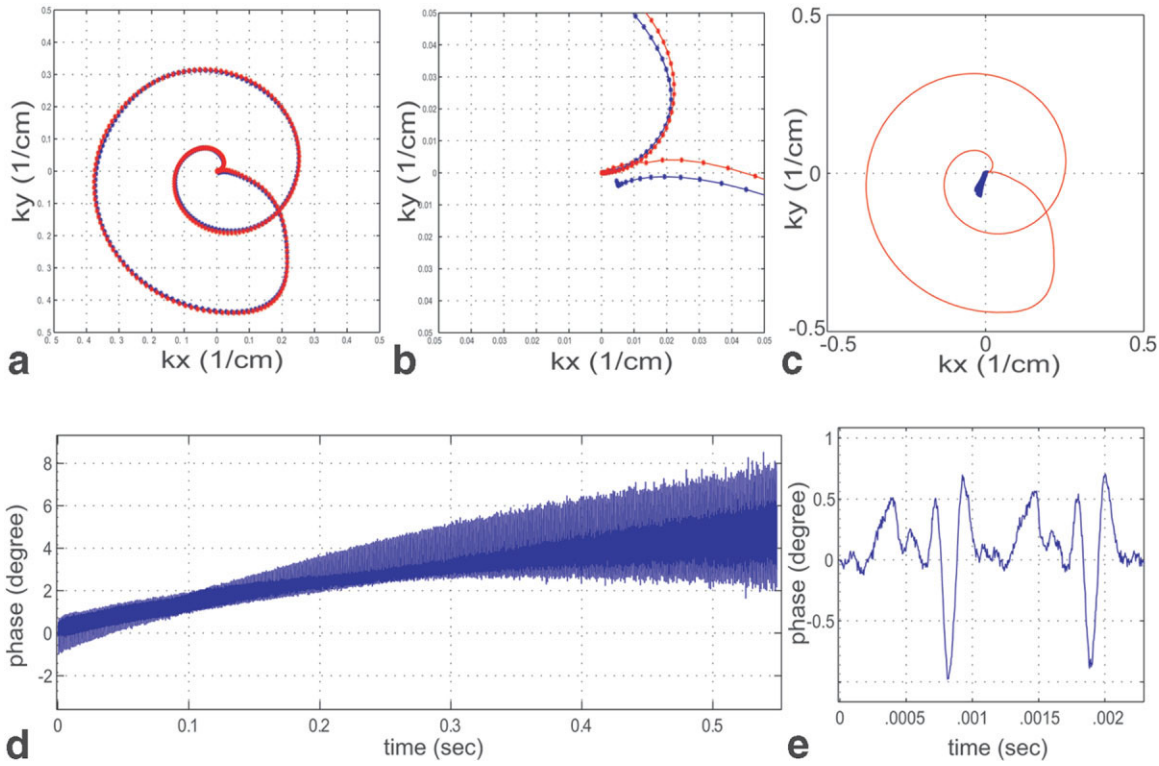

FIG. 1. **a:** Measured *k*-space trajectory (blue) and desired trajectory (red). The discrepancy of the two is further exemplified in **b**. In **c** the desired trajectory (red) is shown, and the difference between the designed trajectory and measured trajectory is shown (blue) over the duration of the entire 512-ms readout. In **d** the $\Delta b(t)$ measured is shown with specific time points in **e**. The main field deviation causes a bulk drift of approximately $\pm 5°$ during the readout interval.

sation is shown. The difference spectra show that there is a small spatially varying frequency term. Although spectra are shown for only one component here, the amount of this spatially varying frequency shift also depends on the component's chemical shift, which implies a spectrally and spatially dependent frequency variation. However, the overall size of this artifact was small compared to the effects caused by the *k*-space distortions.

In Figs. 4 and 5 real data from phantom and in vivo acquisitions are shown. In these images we show the sig-

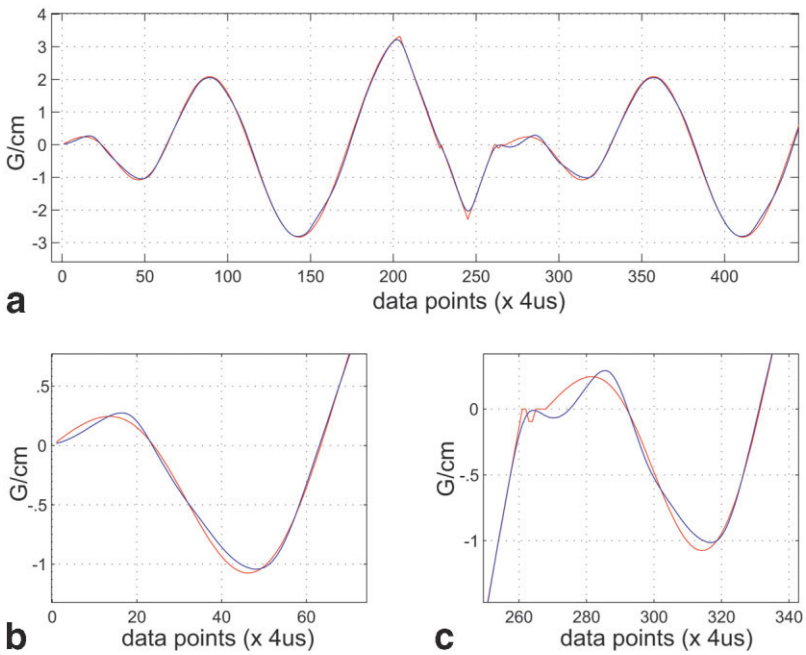

FIG. 2. The effective gradient waveform. Using the measured *k*-space trajectory, the effective gradient that has been executed can be inferred by differentiating $k(t)$ with respect to time. Shown are the designed gradient waveform (red) and the actual gradient waveform (blue) for a small portion of the readout. It can be seen that the actual gradients (blue) lag behind the desired waveform (red). This information can be very useful in gradient design using precompensated trajectories.

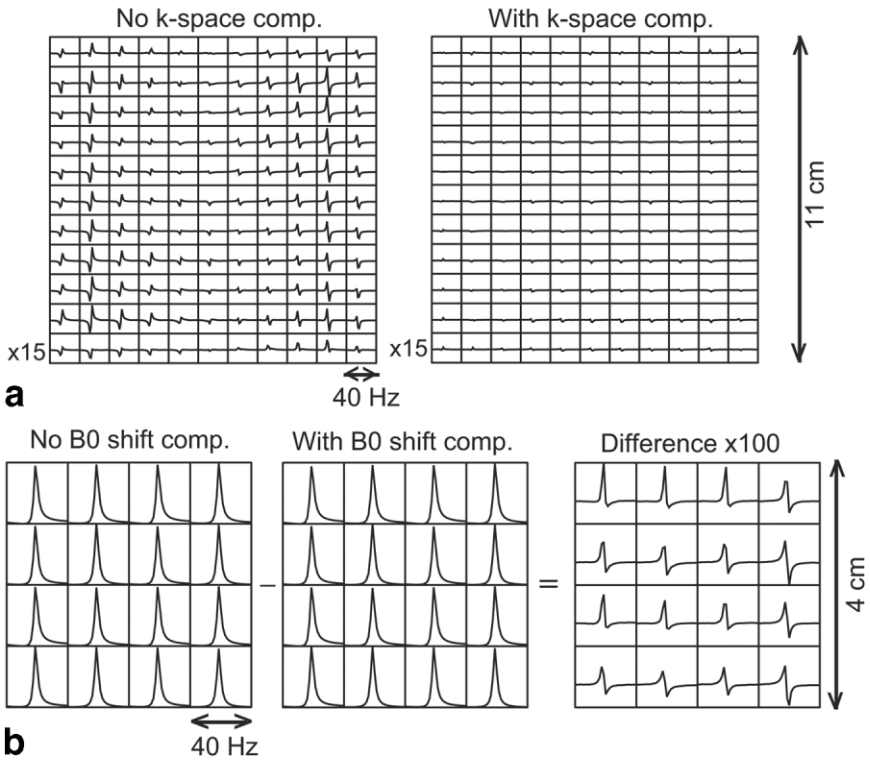

FIG. 3. Simulation results regarding (**a**) *k*-space and (**b**) main field distortions. In a the spectra represent the resulting artifacts obtained when (left) data are acquired on the measured trajectory and reconstructed on the ideal trajectory, and (right) data are acquired on the measured trajectory and reconstructed on the measured trajectory. Using the measured trajectory for the reconstruction results in reduced residual artifacts. The pattern of the residual artifacts (left) shows largely a 1D dependence, which is correlated to the 1D drift of the measured *k*-space trajectory shown in Fig. 1. In b the differences in the reconstructed spectra with (middle) and without (left) main field distortion compensation are shown. The difference shows a spatially varying frequency term. The amount of artifact caused by the main field drift is small compared to the effects caused by the *k*-space trajectory distortions. All voxels shown are within the PRESS volume.

nal level changes in the reconstructed images using corrected and uncorrected trajectories as opposed to the simulations, in which images were reconstructed using raw data from ideal trajectory and ideal data acquisition. This can not be performed for real data. Figure 4 shows results obtained from a phantom. Spectra from several voxels are shown in which the data were reconstructed without (spectra on the left) and with (spectra on the right) the measured trajectories. This comparison shows that using measured trajectories for data reconstruction results in signal amplitude recovery as well as linewidth reduction. Quantitative analysis showed that amplitude recoveries of up to 20% (NAA), 15% (Cr), and 14% (Cho) were achieved for voxels that were severely distorted. Voxels with distortion are similar to those of Fig. 3a.

Figure 5 shows in vivo results. For each location, spectra obtained by reconstructing with the measured trajectory are shown on the top. The difference between reconstruction with the measured trajectory and reconstructing with the designed trajectory are shown on the bottom. The amount of metabolites, representing signal loss without trajectory compensation. The amount of signal loss was as high as 18% for the uncompensated reconstruction. The locations of the voxels showing the most signal recovery for both Figs. 4 and 5 were generally along the anterior–posterior (A/P) direction, similarly to the pattern shown in Fig. 3a.

DISCUSSION

In this work we have shown adverse effects resulting from the undesirable properties of the oscillating readout gradients on spiral MRSI. We demonstrated that the presence of spiral readouts for MRSI results in spatially and spectrally dependent amplitude modulations and frequency shifts. These artifacts are difficult to model using linear system approaches. Therefore, we developed a method that measures the true *k*-space trajectory by assuming distortions in the linear gradients and main field term. For the first time these measurements were acquired over the duration of the entire readout period. The measurement method, which incorporates a PRESS excitation scheme, can be used as an effective tool for checking gradient hardware fidelity and can be readily used for other fast CSI methods, such as EPI-based readouts. We have also shown that using the measured trajectories in the reconstruction process can reduce the artifacts compared to reconstruction without any knowledge of actual trajectories. On our 3 T system, the amount of signal amplitude recovered was up to 20%; however, the amount of improvement depends on the performance of the particular gradient hardware and the specific gradient waveform design.

Although it was shown that the measured trajectories for reconstruction can reduce artifacts, inherent errors in the measurement scheme may arise and add more noise and

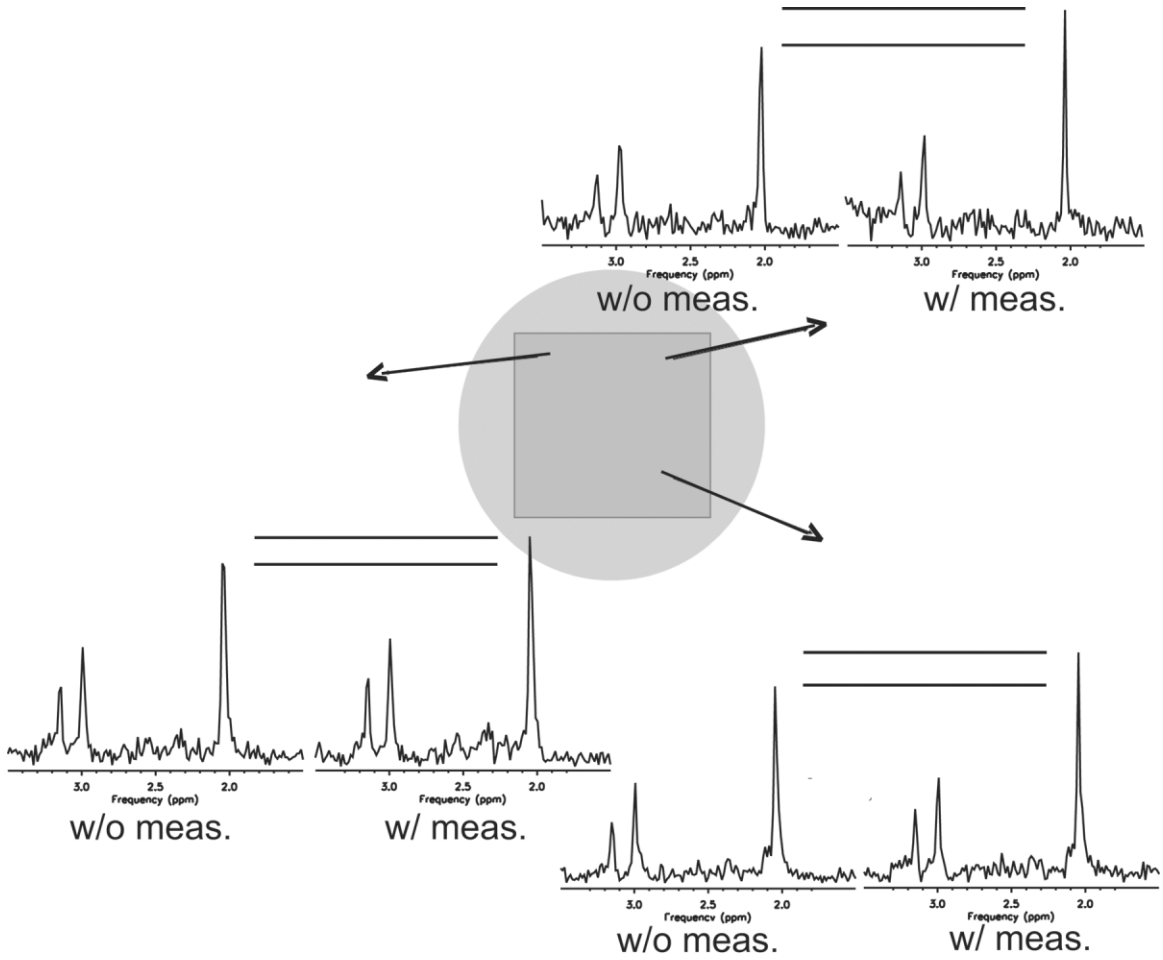

FIG. 4. Experimental results obtained from a phantom. Spectra from voxels where data reconstruction was conducted without (left spectra) and with (right spectra) the measured trajectory compensation are shown. The use of measured trajectories for data reconstruction yields signal amplitude recovery (horizontal lines) as much as 20% (NAA), 15% (Cr), and 14% (Cho). The position of the voxels with the most improvement is tightly correlated with the pattern of distortion of Fig. 3. [Color figure can be viewed in the online issue, which is available at www.interscience.wiley.com.]

further distort the data reconstruction process, resulting in a signal-to-noise ratio (SNR) reduction. Various sources of measurement error exist. One potential error is in the measurement model. We assumed that the majority of distortion results in k-space distortion and main field drift. Although previous studies regarding eddy currents confirmed this assumption, several recent studies have shown that both coupling effects and higher-order terms can be present (14,15). Another source of error is that each measurement is SNR-limited, which fundamentally limits the accuracy. To address this, we chose a relatively long scan time and used a phantom with a long T_2 value (>500 ms). Using this method directly in vivo would require additional scan time for sufficient SNR.

A further question involves the reproducibility of the measurements. This issue arises if the executed gradient trajectory differs each time it is played out, as a result of, e.g., gradient heating. One of the reasons for placing the voxels at various locations was to simultaneously investigate the measurement reproducibility. In our tests, while most of the measured points were fairly well fitted by the linear fit, occasionally there were cases in which a measurement was inconsistent with the other measurements (approximately one in 10 measurements). This data point was not used in the trajectory measurement; however, it can be problematic in an actual scan because the executed trajectory may differ from our measured trajectories. In this case, one must take care in analyzing the reconstructed spectra by comparing the quality obtained with and without measurement compensation.

Finally, in addition to the errors we measured, small field drifts of the main magnetic field (typically below 0.1 ppm/hr) can lead to suboptimal water suppression, line-broadening, and loss of phase coherence in an MRSI examination (16). Although our analysis tool currently does not include this feature, the reconstruction process can readily take it into account. To estimate this drift one can incorporate a method to extract $\Delta b(t)$ at $t = 0$ for each time frame (11).

CONCLUSIONS

In this study we focused on the effects of imperfect gradient properties on spiral MRSI. We demonstrated a

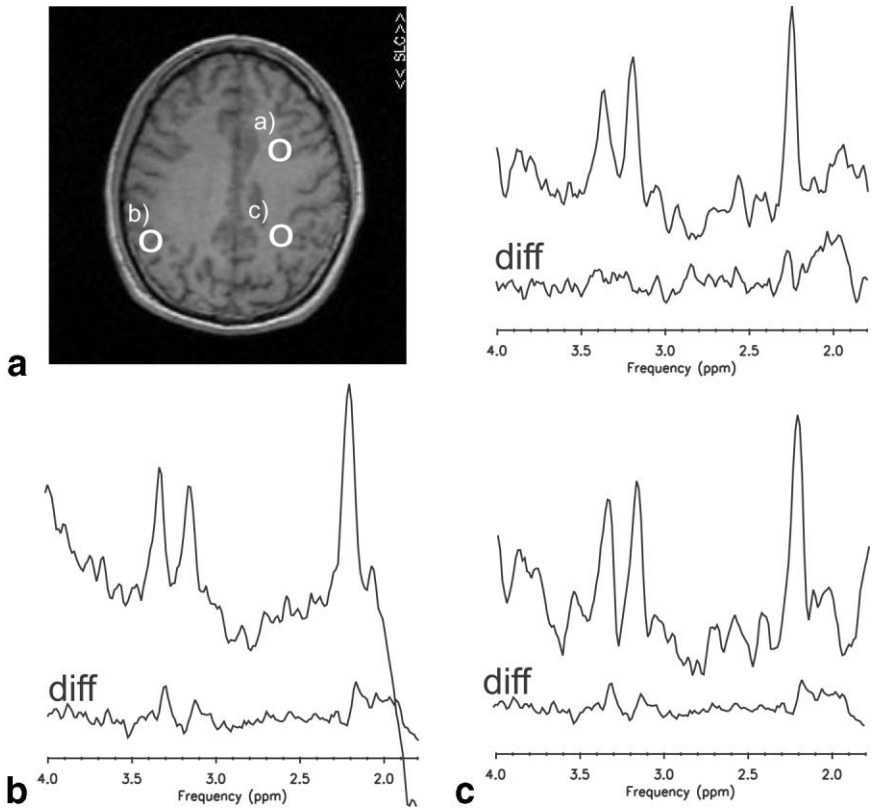

FIG. 5. In vivo results. For each voxel, spectra obtained with reconstruction using the measured trajectory are shown on the top, while the difference between reconstructing with and without the measured trajectory is shown on the bottom. The difference in the spectra shows small positive amounts of metabolite, representing signal loss without trajectory compensation of as much as 18%.

method for reducing these effects using measured trajectories in the reconstruction process. This method can be readily extended to other fast MRSI sequences that incorporate oscillating readout gradients, such as echo-planar MRSI. The method can also be useful for assessing gradient fidelity, and performing routine gradient hardware quality assurance checks.

REFERENCES

1. Adalsteinsson E, Irarrazzabal P, Topp S, Meyer C, Macovski A, Spielman DM. Volumetric spectroscopic imaging with spiral-based k-space trajectories. Magn Reson Med 1998;39:889–898.
2. Onodera T, Matsui S, Sekihara K, Kohno H. A method of measuring field-gradient modulation shapes. Application to high speed NMR spectroscopic imaging. J Phys E: Sci Instrum 1987;20:416–419.
3. Takahashi A, Peters T. Compensation of multi-dimensional selective excitation pulses using measured k-space trajectories. Magn Reson Med 1995;34:446–456.
4. Mason GF, Harshbarger T, Hetherington HP, Zhang Y, Pohost GM, Twieg DB. A method to measure arbitrary k-space trajectories for rapid MR imaging. Magn Reson Med 1997;38:492–496.
5. Papadakis NG, Wilkinson AA, Carpenter TA, Hall LD. A general method for measurement of the time integral of variant magnetic field gradients: application to 2D spiral imaging. Magn Reson Imaging 1997; 15:567–578.
6. Alley MT, Glover GH, Pelc NJ. Gradient characterization using a Fourier-transform technique. Magn Reson Med 1998;39:581–587.
7. Duyn JH, Yang Y, Frank JA, van der Veen JW. Simple correction method for k-space trajectory deviations in MRI. J Magn Reson 1998; 132:150–153.
8. Liu Q, Hughes DG, Allen PS. Quantitative characterization of the eddy current fields in a 40-cm bore superconducting magnet. Magn Reson Med 1994;31:73–76.
9. Papadakis NG, Martin KM, Pickard JD, Hall LD, Carpenter TA, Huang CLH. Gradient preemphasis calibration in diffusion-weighted echo-planar imaging. Magn Reson Med 2000;44:616–624.
10. Klose U. In vivo proton spectroscopy in presence of eddy currents. Magn Reson Med 1990;14:26–30.
11. Ebel A, Maudsley AA. Detection and correction of frequency instabilities for volumetric 1H echo-planar spectroscopic imaging. Magn Reson Med 2005;53:465–469.
12. Kim DH, Adalsteinsson E, Spielman D. Spiral readout gradients for the reduction of motion artifacts in chemical shift imaging. Magn Reson Med 2004;51:458–463.
13. Glover GH. Simple analytic spiral k-space algorithm. Magn Reson Med 1999;42:412–415.
14. Ahn CB, Zho ZH. Analysis of the eddy current induced artifacts and the temporal compensation in nuclear magnetic resonance imaging. IEEE Trans Med Imaging 1991;10:47–52.
15. Lee SW, Lee G, Olafsson V, Noll DC. A k-space measurement technique with single point excitation. In: Proceedings of the 13th Annual Meeting of ISMRM, Miami Beach, FL, USA, 2005. p 792.
16. Thiel T, Czisch M, Elbel GK, Hennig J. Phase coherent averaging in magnetic resonance spectroscopy using interleaved navigator scans: compensation of motion artifacts and magnetic field instabilities. Magn Reson Med 2002;47:1077–1082.